BBA - General Subjects 1862 (2018) 1079–1090

Contents lists available at ScienceDirect

BBA - General Subjects

journal homepage: www.elsevier.com/locate/bbagen

The relative composition of actin isoforms regulates cell surface biophysical features and cellular behaviors

Xin Xie[a,1], Muhammedin Deliorman[b,1], Mohammad A. Qasaimeh[b,c], Piergiorgio Percipalle[a,d,*]

[a] Science Division, Biology Program, New York University Abu Dhabi (NYUAD), P.O. Box 129188, Abu Dhabi, United Arab Emirates
[b] Engineering Division, New York University Abu Dhabi (NYUAD), P.O. Box 129188, Abu Dhabi, United Arab Emirates
[c] Department of Mechanical and Aerospace Engineering, New York University, USA
[d] Department of Molecular Biosciences, The Wenner-Gren Institute, Stockholm University, SE-106 91 Stockholm, Sweden

ARTICLE INFO

Keywords:
β-actin
Actin isoforms
Membrane properties
Membrane tension
Cell behavior
Transcriptomics

ABSTRACT

Background: Cell surface mechanics is able to physically and biomechanically affect cell shape and motility, vesicle trafficking and actin dynamics. The biophysical properties of cell surface are strongly influenced by cytoskeletal elements. In mammals, tissue-specific expression of six actin isoforms is thought to confer differential biomechanical properties. However, the relative contribution of actin isoforms to cell surface properties is not well understood. Here, we sought to investigate whether and how the composition of endogenous actin isoforms directly affects the biomechanical features of cell surface and cellular behavior.

Methods: We used fibroblasts isolated from wild type (WT), heterozygous (HET) and from knockout (KO) mouse embryos where both β-actin alleles are not functional. We applied a combination of genome-wide analysis and biophysical methods such as RNA-seq and atomic force microscopy.

Results: We found that endogenous β-actin levels are essential in controlling cell surface stiffness and pull-off force, which was not compensated by the up-regulation of other actin isoforms. The variations of surface biophysical features and actin contents were associated with distinct cell behaviors in 2D and 3D WT, HET and KO cell cultures. Since β-actin in WT cells and smooth muscle α-actin up-regulated in KO cells showed different organization patterns, our data support the differential localization and organization as a mechanism to regulate the biophysical properties of cell surface by actin isoforms.

Conclusions: We propose that variations in actin isoforms composition impact on the biophysical features of cell surface and cause the changes in cell behavior.

1. Introduction

Actin cytoskeleton is the major filamentous network which functions to dynamically control cell polarity, membrane dynamics, cell movement and nuclear organization in eukaryotic cells [1,2]. In mammals, six actin isoforms are expressed in a tissue-specific manner, varying from the well-organized contractile apparatus consisting of skeletal muscle α-actin to the highly versatile actin cytoskeleton containing β-actin and γ-actin in non-muscle cells [3]. Functional studies of actin isoforms using knockout mice demonstrate distinct phenotypes, implying tissue-specific roles of each isoform in development [4]. Rescue experiments further reveal the functional convergence or divergence of specific isoforms. For example, transgenic expression of cardiac α-actin can fully rescue the lethality and muscle defects of skeletal α-actin knockout mice [5]. However, the expression of cytoplasmic γ-actin fails to rescue the lethality of skeletal α-actin knockout, even though the forced expression of γ-actin in wild-type can substitute 40% of skeletal α-actin in muscle thin filament [6]. Interestingly, in all knockout mouse models, there is a compensatory up-regulation of a subset of other actin isoforms [7], suggesting preferential functional interactions of certain isoforms.

Different tissues have different biomechanical properties corresponding to their physiological functions. There is evidence that actin cytoskeleton dynamics and alignment are linked to tissue-specific mechanical properties [8]. For example, myoblasts (C2C12 cells), which usually take an elongated shape, are more sensitive to growth geometry change than endothelial cells (HUVECs) or fibroblasts (NIH 3T3 cells) [9]. This is associated with specialized α-actin arrangement in elongated muscle cells. It is therefore likely that actin isoforms with specific subsets of actin-binding proteins contribute differentially to the

* Corresponding author at: Science Division, Biology Program, New York University Abu Dhabi (NYUAD), P.O. Box 129188, Abu Dhabi, United Arab Emirates.
E-mail address: pp69@nyu.edu (P. Percipalle).
[1] Equal contribution.

https://doi.org/10.1016/j.bbagen.2018.01.021
Received 12 October 2017; Received in revised form 28 January 2018; Accepted 31 January 2018
Available online 02 February 2018
0304-4165/

mechanical properties of the cell [4], by regulating the biophysical properties of specialized organelles such as membranes. This in turn is likely to impact on cellular behavior.

Biophysical properties of cell surface can influence a variety of cellular processes and behaviors, because cell surface mechanics is related to the force or tension during membrane deformation in cell migration and tissue morphogenesis [10–12]. Cell surface features such as actin cortex mechanics control animal cell shape [13]. Additionally, mechanical stimuli from cell surface can impact on a variety of cellular processes inducing cell shape change, migration and differentiation [14]. Change in cell surface tension such as exposure to osmotic stress also induces actin cortex reorganization [15]. It is known that cell membrane tension and bending stiffness is strongly influenced by cytoskeletal elements [16–20]. However, the relative contribution of individual actin isoforms to cell surface mechanics has not been investigated.

In this study, we sought to investigate whether and how the composition of endogenous actin isoforms directly affects the biomechanical features of cell surface and cellular behaviors. For this, we used fibroblasts isolated from wild type (WT) mouse embryos (β-actin$^{+/+}$) as well as from heterozygous (HET) mouse embryos with only one functional β-actin allele (β-actin$^{+/-}$) and from knockout (KO) mouse embryos where both β-actin alleles are not functional (β-actin$^{-/-}$) [21]. Transcriptome analysis of the three cell types showed that WT, HET and KO cells expressing different amounts of β-actin mRNA exhibit varying levels of other actin isoforms such as smooth muscle α-actin and cytoplasmic γ-actin mRNAs. Endogenous β-actin in WT cells and the smooth muscle α-actin up-regulated in KO cells show different organization patterns. Interestingly, in HET and KO cells loss of β-actin leads to a decrease in cell surface stiffness and an increase of surface pull-off force in comparison to WT cells, indicating an essential role of β-actin in controlling cell surface biophysical properties. This is further supported by the observation that expression of exogenous β-actin in KO cells increases cell surface stiffness. The changes of biophysical properties of cell surface were associated with distinct cellular behaviors in 2D and 3D cultures among WT, HET and KO cells. Taken together, we show that variations in the composition of actin isoforms impact on cell surface mechanics, leading to changes of cellular behaviors.

2. Materials and methods

2.1. Antibodies and reagents

Anti-mouse IgG Alexa Fluor 647 (ab150115), Anti HA antibody (ab9110), Phalloidin-iFluor555 (ab176756), Y-27632 dihydrochloride (ab120129) were from Abcam. Antibody against β-actin (clone AC-74) was from Sigma-Aldrich. Antibodies of smooth muscle α-actin (α-SMA) (MA5-11547), rabbit IgG Dylight 550 (84541), mouse IgG Dylight 550 (84540), Hoechst 43222 (H1399), Wheat Germ Agglutinin (WGA) Alexa Fluor 647 conjugate (W32466) were purchased from Thermal Fisher Scientific. Cultrex 3D culture matrix rat collagen I (3447-020-01) is from R&D systems. Propidium iodide solution (J66584) was purchased from Alfa Aesar.

2.2. Cell culture

The β-actin$^{+/+}$ MEFs (WT), β-actin$^{+/-}$ MEFs (HET) and β-actin$^{-/-}$ MEFs (KO), and mouse endothelial cell line C166 (ATCC) were maintained and cultured with Dulbecco's modified Eagle medium (DMEM) with high glucose (Sigma), 10% fetal bovine serum (Sigma) and 100 units/mL penicillin and 100 μg/mL streptomycin (Sigma), in a humidified incubator with 5% CO_2 at 37 °C. For AFM measurement, fibroblast was seeded on glass slide and cultured in CO_2-independent L-15 Medium (Leibovitz, Sigma) supplemented with 1× GlutamMAX, 10% fetal bovine serum (Sigma) and 100 units/mL penicillin and 100 μg/mL streptomycin (Sigma).

2.3. Atomic force microscopy (AFM)-based force measurements

Fibroblasts were cultured on fibronectin-coated microscope glass slides for overnight in L-15 Leibovitz medium. All AFM measurements, lasting no > 3 h per experiment, were performed with 5500 AFM from Keysight Technologies using ~6 μm-diameter colloidal silicon spherical tips, which are attached to cantilevers with 0.08 N/m nominal spring constants. The tips were uncoated while the detector sides of the cantilevers were coated with ~70 nm gold (CP-PNPL-SiO-C-5 from NanoAndMore, Germany). Custom gold-coated silicon chips covered with hydrophobic Teflon membranes were used as “liquid cells”. The cantilever spring constants were determined from the power spectral density of the thermal noise fluctuations [22] before each experiment. Tip approach and retract velocity was set at ~5 μm/s. Prior to any measurements, cells of interest were carefully located using a video camera attached to the system (Fig. S2A, upper inset). Once cells have been located, force measurements were performed in the force-volume (FV) mode, in which the approach-retraction process (Fig. S2A) is repeated over cells, at a resolution of 8 × 8 pixels per FV image. For each set of experiment, the AFM probe was aligned at the center of a cell and subsequently 64 pairs of force versus displacement curves were acquired from a 10 × 10 μm^2 cell surface area in the FV mode. The force curves on all the pixels in the FV image were then analyzed with a home-made software [23] to obtain the distribution of the elasticity and maximum pull-off forces, as explained in detail below. Force profiles with unclear approach and/or retraction curves were excluded from the analysis. The number of investigated cells were 19, 17, 17, 20, and 18 cells for WT, KO, HET, KG, and KA, respectively. Every culture sample was measured using a new tip.

Quantitative information on cell elasticity was obtained by modeling the measured loading force versus surface indentation data using the classic Hertz model of contact mechanics [24]. According to the model, the loading force (F_L) applied by a non-deformable sphere indenter (the AFM tip) required to indent a distance (δ) into an infinitely deformable elastic half space (the cell surface) is given by:

$$F_L = \frac{4}{3}\frac{E}{(1-\nu^2)}R^{1/2}\delta^{3/2} \quad (1)$$

where E is the Young's modulus (i.e. elasticity modulus) of the cell, R is the radius of the spherical indenter, and ν is the Poisson ratio of the cell, which was set to 0.5 assuming cell's incompressibility. All force measurements were performed under a trigger force of about 1.5 nN, which reflected a cell surface indentation of approximately 2 μm. Fit range was chosen to be 400 nm (Fig. S2A, lower inset). The adhesion forces, comprising all interaction forces (specific and nonspecific) between the tip and cell surface, are defined as pull-off forces [25]. Quantitative analysis on maximum pull-off force was performed by first identifying local minima events on the retraction curves. In addition, force curves that possessed pull-off force values below 10 pN cut-off force were discarded from the analysis due to experimental noise during measurements. The data sets taken on WT cells in 64 × 64 pixel-resolution FV mode served as control of how the maximum pull-off forces are distributed over the cells interacting with AFM tip (Fig. S2C). Origin software (OriginLab, Northampton, MA) was used to evaluate the arithmetic mean and the standard deviations of the histograms by fitting the data to the LogNormal or Gauss probability density functions. This way, the average elasticity/maximum pull-off force based on the total number of indentation locations and adhesion/tether events investigated for cells of each condition were identified, which are expected to yield accurate estimate [26]. Unless otherwise specified, all the quantitative analysis related to elasticity and adhesiveness properties was conducted from the same set of force data collected on the cells.

2.4. RNA-sequencing analysis

Total RNA was extracted from 70% confluent cells using TRI Reagent according to the manufacturer protocol (Sigma-Aldrich). Quality of total RNA were re-evaluated at SciLIfe lab (Stockholm, Sweden) using Qubit and Bioanalyzer respectively, samples which pass the QC were used for library construction according to the SciLife lab guideline using TruSeq Stranded mRNA Library Prep Kit (Illumina). Deep sequencing was performed at Science for Life Laboratory, the National Genomics Infrastructure, NGI, Karolinska Institute, Stockholm. RNA-seq data was processed through the standard RNAseq analysis pipeline at NYUAD. RNA-seq data was deposited in GEO repository and the GEO accession number is GSE95830.

2.5. Flow cytometry analysis

For phalloidin staining, cells were fixed with 4% formaldehyde and then permeabilized with 0.5% Triton X100 in PBS for 15 min. Cells were stained with 1X phalloidin-iFluor 555 (Abcam) for 30 min. Stained cells were washed 3 times in cold PBS before FACS analysis. For intracellular staining, fixed cells were permeablized with 0.5% Triton X100 for 15 min. Cells were blocked with 1% BSA for 30 min and stained with β-actin antibody (1:250) and α-SMA antibody (1:100) for 1 h. After 3 washes with permeabilization buffer, cells were stained with anti-mouse IgG Dylight 550 (1:1000) for 1 h. After 3 washes, stained cells were re-suspended in PBS and analyzed by FACS. For hypo-osmotic stress assay, cells pulsed with sterile distilled water (Stress) or PBS (Mock) for 3 min. After recovery in fresh medium for 1 h, both the floating and adhering cells were collected and stained with 2.5 μg/mL propidium iodide in PBS for 10 min. The stained cells were subject to FACS analysis. Data from flow cytometer BD FACSAria II were analyzed using Flow Jo software.

2.6. Immunostaining

Cells grown on poly-L-lysine or fibronectin-coated glass cover slip were cultured in DMEM or L-15 medium. Cells were fixed by cold 70% ethanol for 10 mins and then permeabilized with 0.5% Triton X-100 for 15 min. After blocking in 1% BSA for 1 h, cells were stained with anti-HA (1:200), anti-α-SMA (1:100) or anti-β-actin (1:200) for 2 h. Then cells were washed 3 times with TBST buffer, followed by staining with corresponding secondary antibody (1:1000) and Hoechst 43,222 (1:6000) for 1 h. Stained cells were observed using Olympus FV1000 confocal microscope.

2.7. Cell morphology analysis by high-content profiling platform

MEFs were cultured in 96-well plate (Corning), at density of 5000 cells/well. Cells were fixed by 3.7% formaldehyde and the cell membrane were labeled with WGA Alexa Fluor 647 (10 μg/mL) for 15 min. After 3 times wash with PBS, stained cells in plate were scanned via Cellomics ArrayScan™ XTI High Content Analysis (HCS) platform (Thermo Fisher Scientific), with a 20× Objective. Compartment Analysis Bio Application software (Cellomics) was applied to automatic image analysis. For each experiment, at least 500 valid cells (single cells) per culture well were analyzed in at least 10 independent culture wells. For the cell spreading assay, trypsinzed cells were seeded to 96-well plates at about 6000 cells/well. 15 min were allowed for cell settlement at the bottom. Then cells were fixed at different time points and then stained with WGA membrane dye. Same image analysis was applied to determine cell area at different time points.

2.8. 3D collagen gel cell culture

2.5×10^5 cells in 400 μL DMEM supplemented with 10% FBS were mixed with 200 μL Rat Collagen I solution at 3 mg/mL. Then 6 μL NaOH at 1 M was added to neutralize the PH to initiate gel polymerization. After brief mixing, the cell and gel mixture was transferred to 24 well-plate to allow the collagen gel to solidify at 37 °C for 15 mins. Then 500 μL fresh DMEM (10% FBS) were added and the gel was detached from the well using sterile pipette tips. The whole well image of the gel was collected by Nikon SMZ18 stereomicroscope. The morphology of the cells in the gel matrix was collected by Olympus FV1000 confocal microscope. The relative gel surface area and cell protrusion was measured by ImageJ software.

2.9. Real-time qPCR

Total RNA was extracted using RNeasy Mini Kit (Qiagen) according to the manufacturer's instruction. 1 μg total RNA was reverse transcribed to cDNA by RevertAid First Strand cDNA synthesis Kit (Thermo Fisher Scientific). Diluted cDNA was subjected to quantitative real-time PCR analysis using Maxima SYBR Green qPCR Mix (Thermo Fisher Scientific) on Stratagene 3005 qPCR system (Agilent Technology). All the target gene expression level was normalized to the expression of *Nono* reference gene. Primers used: *Actb* primers: Forward: TATCGCT GCGCTGGTCG; Reverse: CCCACGATGGAGGGGAATAC. *Nono* Primers: Forward: GCCAGAATGAAGGCTTGACTAT; Reverse: TATCAGGGGGAA GATTGCCCA.

2.10. Retrovirus production and cell transduction

Retrovirus vector, virus preparation and cell transduction were performed as described previously [27]. Mouse β-actin cDNA was cloned from cDNA of the WT MEF and ligated into a retrovector with rCD8a as transduction marker [27]. Virus supernatant was produced by transfecting 293T cells with equal amounts of retroviral vector and pCL-Eco packaging plasmid (Novus Biologicals) using the Phosphate Transfection Kit (Invitrogen). Supernatant of transfected cells was collected at 48 h and 72 h post-transfection and was snap-frozen in liquid nitrogen and stored at −20 °C. For retroviral transduction, MEF cells in 96 well plate were incubated with 100 μL medium and 100 μL viral supernatant, with 8 μg/mL polybrene. The cells culture were centrifuged at 2500 rpm for 1.5 h at 32 °C and then transferred to incubator. After 12 h, fresh culture medium were added for another 24 h incubation. Cells after expansion were stained with anti-rat CD8a-PE antibody (1:200 in PBS with 5 mM EDTA) for 15 min. Stably transduced rCD8a + cells were sorted by FACS (BD FACSARIA III) and expanded in DMEM with 20% FBS.

2.11. Statistical analysis

To compare the statistical significance of one variable between two cell types, two-tailed Student's *t*-test was applied. For gene expression levels comparison, Student's *t*-test was applied between two cell types, although there are 3 cell types together. This is because the gene expression level of one cell type is too far away from the other two cell types, so the obvious biological difference between the other two cell types will be statistically insignificant if One-Way ANOVA is applied. For multiple comparisons under experimental conditions, One-Way ANOVA was applied to compare the changes among three or more different samples for a single variable factor. Two-Way ANOVA was used when two variable factors exist for multiple sample comparison. For both One-Way and Two-Way ANOVA, Bonferroni Post Hoc Test was used to get the statistic *p*-values. All biological experiment data were analyzed by GraphPad Prism 5 software and are shown as Mean ± S.E.M. (Standard Error of Mean). Values of AFM experiments generated by Origin software are displayed as Mean ± SD (Standard Deviation).

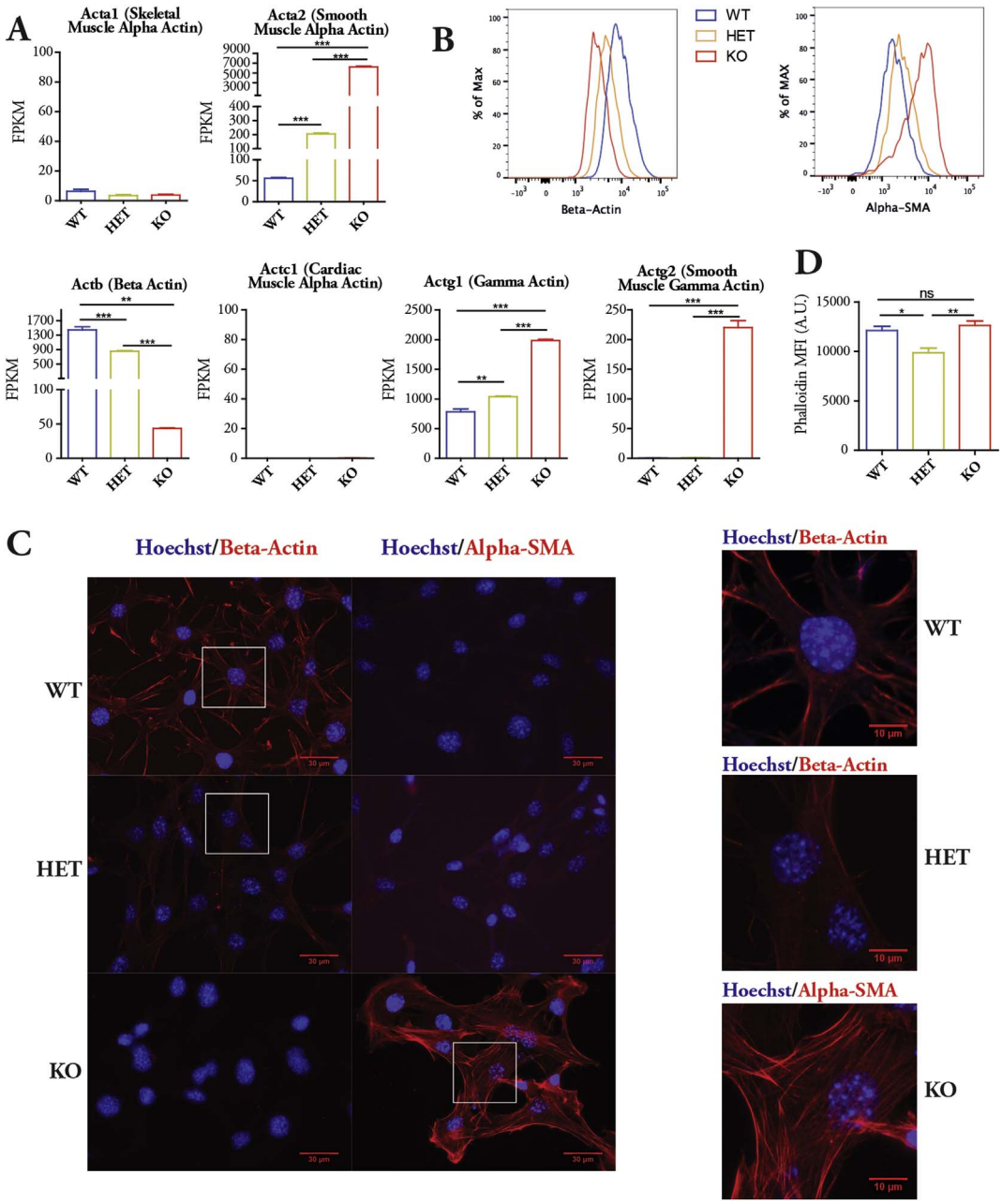

Fig. 1. A cellular model with different actin isoform composition. A. Transcript levels (FPKM) of all known actin isoforms in β-actin$^{+/+}$ MEFs (WT), β-actin$^{+/-}$ MEFs (HET) and β-actin$^{-/-}$ MEFs (KO) from RNA-sequencing analysis. Student's *t*-test: (**) $p < 0.01$. (***) $p < 0.001$, Mean ± S.E.M. **B.** FACS analysis of intracellular staining of β-actin and α-SMA in WT, HET and KO MEFs. Data is representative of two independent experiments. **C.** WT, HET and KO MEFs were fixed on glass slide and stained with β-actin and α-SMA antibodies respectively. Right panel shows enlarged images of selected region of the left panel. Data is representative of three independent experiments. **D.** WT, HET and KO MEFs were stained with Phalloidin-iFluro 555 and analyzed by FACS. Mean Phalloidin fluorescence intensity of three independent experiments were shown. One-way ANOVA analysis with Bonferroni Post Hoc Test: (*) $p < 0.05$; (**) $p < 0.01$, Mean ± S.E.M.

3. Results

3.1. Cellular models with different compositions of specific actin isoforms

Previous studies have shown that changes in β-actin or γ-actin levels lead to compensatory up-regulation of other actin isoforms [21,28]. In this study, we used the recently characterized WT β-actin$^{+/+}$ MEFs, HET β-actin$^{+/-}$ MEFs and KO β-actin$^{-/-}$ MEFs to study how β-actin specifically contributes to biophysical features of cell surface. To study whether total mRNA expression levels of different actin isoforms are altered in the absence of β-actin, four biological replicates of total RNA isolated from each cell type were subject to deep sequencing. The transcript levels of actin genes were normalized and expressed in FPKM (Reads per kilobase of exon per million reads mapped). As expected, *Actb* (β-actin) transcript levels were reduced in HET cells and also in KO cells, although in KO cells the transcript was not completely lost (Fig. 1A). This is a direct consequence of the insertional nature of the knockout system where the *Actb* gene is disrupted but still present in KO cells [29]. Using intracellular staining and FACS analysis, we confirmed that in KO cells β-actin protein expression was not detected whereas HET cells showed intermediate protein levels compared to WT cells (Fig. 1B, Fig. 1C). In contrast, results from transcriptional profiling and analysis of differential gene expression patterns revealed that smooth muscle α-actin (α-SMA) *Acta2* and cytoplasmic γ-actin *Actg1* mRNA levels were significantly increased concomitantly with the decrease of β-actin level, although to different extents when comparing HET and

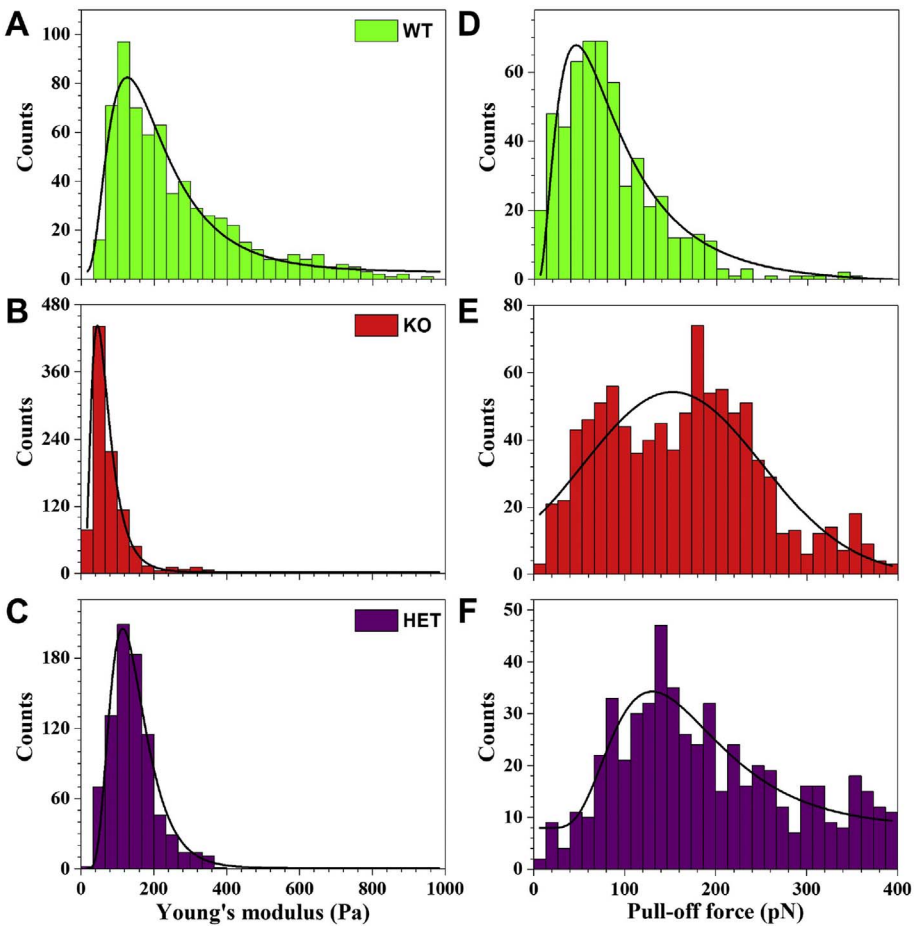

Fig. 2. Cell membrane elasticity and adhesiveness analysis. Histograms of the distribution of all Young's moduli (A–C) and maximum pull-off force (D–F) measured for WT, KO, and HET cells. Each count in the data represents an individual measurement event by the AFM tips. Data are pooled results from three independent experiments. Solid black lines are LogNormal or Gauss fit to data.

KO cells (Fig. 1A). Smooth muscle γ-actin *Actg2* mRNA was not detectable in the presence of β-actin but its levels are greatly up-regulated in KO cells (Fig. 1A). Under the same conditions, changes in gene expression patterns were not observed for cardiac muscle α-actin *Actc1* mRNA and skeletal muscle α-actin *Acta1* mRNA, both showing very low expression in all 3 cell types (Fig. 1A). Together, these data show that β-actin expression affects expressions of smooth muscle α-actin *Acta2*, cytoplasmic γ-actin *Actg1* and smooth muscle γ-actin *Actg2* genes in a dosage-dependent manner.

We next examined the cellular distributions of β-actin and α-SMA in WT, HET and KO cells. Cells were seeded on poly-L-lysine coated glass slip in DMEM medium. The immuno-staining analysis demonstrates that the β-actin fibers in WT cells were predominantly localized at the membrane, similarly to HET cells although in this case with reduced expression (Fig. 1C). In contrast, the α-SMA formed massive fibers across the whole cell body in KO cells (Fig. 1C). The low level of α-SMA in WT and HET cells did not form observable fibers. The distribution and organization pattern of β-actin and α-SMA remain the same when the cells were cultured on fibronectin-coated glass slip with a CO2-independent L-15 medium (Fig. S1). FACS analysis of phalloidin staining demonstrated that HET cells had an overall lower amount of F-actin than WT and KO cells (Fig. 1D). Collectively, β-actin and α-SMA showed different organization pattern.

Seeing that β- to α-actin cellular ratios vary from WT to HET and KO MEFs and that these cells accordingly exhibit different organization patterns of actin isoforms, we propose that these cells altogether provide an ideal model to investigate how the composition of actin isoforms impacts on mechanical features at cell surface.

3.2. Changes in the composition of actin isoforms lead to alterations in cell surface stiffness, pull-off force and indentation properties

Based on the above considerations, we next studied whether WT, HET and KO cells display changes in their surface mechanical properties. In particular, we applied atomic force microscopy (AFM) to quantitatively measure potential differences in cell elasticity and surface pull-off forces of WT, HET and KO cells at single cell level. The pull-off force is defined as the sum of specific and nonspecific interaction forces between the tip and cell surface [25]. Cells seeded on fibronectin-coated glass slip were cultured in CO_2-independent L-15 medium, which is designed for experiment on live cells in CO_2-independent environment. Colloidal probes with a known spherical geometry were used. This facilitated the modeling of the force-indentation data given in Eq.(1) (see Materials and methods). In addition, the use of micron-size colloidal probes allowed for larger areas of the cells to be scanned for their elasticity properties, thus providing in each case a better statistical sampling of the heterogeneous cell surface. In our analysis, we calculated the Young's modulus by fitting the force data for up to 400 nm surface indentations (Fig. S2A, lower inset). An example of high resolution Young's modulus map of WT cell surfaces revealed that the stiffer regions (up to ~644 Pa) were located in the middle parts of the cell body, while less stiff parts were distributed towards the edges of the cell (Fig. S2B). It is important to note that, the loading forces distributed over cell surfaces during indentation experiment varied between ~27 pN and ~516 pN, with a mean value at 130.4 ± 7.4 pN (Fig. S2A). Despite such large loading force variations, surface indentations distributed over cells were uniform (Fig. S3A, Fig. S3B), suggesting the heterogeneity of different cell area of withstanding mechanical force. To study the cell surface pull-off force, the AFM tip was first brought into contact with the cell and then withdrawn. In this

Table 1
Summary of AFM Young's modulus (E) and maximum pull-off force (F_P) measurements for mouse embryonic fibroblasts.

Cell type†	Young's modulus		Pull-off force	
	E (Pa)	No. of locations	F_P (pN)	No. of events
WT	185.3 ± 8.8	649	79.8 ± 8.1	539
KO	57.3 ± 1.5	960	152.6 ± 8.2	939
HET	136.8 ± 2.9	825	160.2 ± 11.5	556

†: The number of investigated cells were 19, 17, and 17 cells for *WT*, *KO*, and *HET*, respectively. Peak values and standard deviations were derived from distribution histograms by using LogNormal or Gauss probability density function. For each set of experiment, 64 pairs of force versus displacement curves were acquired from single cells in the force-volume mode. Data represents mean ± S.D.

approach, the AFM tip is detached from the cell by unloading the applied force through the AFM cantilever at the direction of the cell. During this process, a pair of force versus displacement curve is recorded from which maximum pull-off force is quantified by monitoring the normal deflection of the AFM cantilever in the retraction curve (Fig. S2A). This method is limited to study the cell surface pull-off force at very initial stage because the tip–cell contact time is usually < 1 s with such experimental setup. An example of recorded pull-off force distribution over WT cell was shown in Fig. S2C.

We performed the above analysis for all cell types. The overall distributions of Young's modulus values of WT, KO, and HET cells are presented in Fig. 2A–C. We found that WT cells showed a wide range distribution of elastic phenotypes, with higher Young's modulus values detected than HET and KO cells (Fig. 2A–C). Overall, WT cells displayed more rigid cell surface (185.3 ± 8.8 Pa) when compared to KO (57.3 ± 1.5 Pa) and HET (136.8 ± 2.9 Pa) cells (Table 1). Interestingly, HET cells with only one functional copy of the β-actin alleles exhibited an average 26% decrease of surface stiffness in comparison to WT cells. In KO cells, although there is a heavy up-regulation of *Acta2* and *Actg2* to compensate for the loss of β-actin, surface stiffness dropped by 69% on average in comparison to WT cells (Table 1). Therefore, our data revealed a positive correlation between endogenous β-actin levels and cell surface rigidity, indicating an essential role of β-actin in controlling cell surface elasticity. The loading forces necessary to indent cell surface up to 400 nm in the three cell types were compatible with the corresponding surface stiffness (Fig. 3A–C).

Additionally, there is significant difference in the ranges of surface indentation distances among the 3 cell types. Irrespective of the loading forces applied, HET and KO cells showed wider range of surface indentation than WT cells (Fig. 3D–F), implying a higher degree of heterogeneity of cell surface mechanics in HET and KO cells. Analysis of the maximum surface pull-off forces of KO and HET cells showed broader distributions, and an overall lower pull-off force was detected in WT cells when compared to HET and KO cells (Fig. 2D–F). On average, the surface pull-off force increased by 2-fold in HET and KO cells in comparison with WT cells (Table 1).

Collectively, these data demonstrate that WT, HET and KO MEFs exhibit significant changes in the biomechanical properties of cell surface, which are a likely consequence of different actin compositions and actin cytoskeleton organizations in the three cell types.

3.3. Cellular morphology and adaptability to hypo-osmotic stress change in the varying dosage of β-actin

Alterations in the biophysical features of cells are known to influence their shape and behaviors [30]. Microscopy images showed the morphology of WT, HET and KO cells (Fig. 4A). Given the mechanical differences observed by AFM, we next sought to quantitatively analyze differences in cell shapes among WT, HET and KO cells. Cells were stained with wheat germ agglutinin (WGA membrane stain) and imaged in ArrayScan XTI high content profiling platform. Cell outlines were defined by the membrane staining and the morphology parameters of the valid single cells (cells highlighted with blue outlines) were assessed quantitatively (Fig. S4A). On average, we found that HET and KO cells showed significantly larger areas than WT cells, and that HET cells had a more elongated morphology compared to both WT and KO cells (Fig. 4B, Fig. 4C). The greater Perimeter^2/Area ratio (P2A) value of HET and KO cells indicates that their cellular shape are more complex and deviated from a regular circle than that of WT cells (Fig. 4D).

To test how mechanical stress affects the plasma membrane integrity, we challenged WT, HET and KO cells with hypo-osmotic stress which can cause the rapid increase in cell volume due to the low osmotic surrounding environment. After short pulse with ddH_2O, more HET and KO cells turned into round shape (Fig. S4B). To quantify the cells losing membrane integrity, cells were stained with membrane-impermeable DNA dye *propidium iodide* (*PI*). We found that KO cells were most sensitive to hypo-osmotic stress, as evidenced by the highest percentage of PI + cells with compromised membrane (Fig. 4E, Fig. 4F), whereas HET cells showed intermediate resistance somewhere between WT and KO cells.

Together, these data suggest that actin composition can affect cell shape and the membrane strength under osmotic stress, which might be related to both the cell surface elasticity and cytoskeleton arrangement underlying the membranes.

3.4. Actin compositions differentially contributes to cell spreading

We next sought to investigate how cells with different biophysical features behave in 2D cultures. For this, WT, HET and KO cells were trypsinized and then seeded in 96-well culture plate at low density. After settlement, the cells were followed from 0 h to 6 h in culture to check their rate of spreading out to fibroblast shape. Remarkably, HET cells showed considerably slower rate of spreading out compared to WT and KO cells. At 1 h and 2 h time point, nearly all WT and most of KO cells already showed flattened shape and increased cell size, while most HET cells remained round-shaped or just began to stretch out (Fig. 5A). Cells fixed at different time points were, then, stained with WGA membrane dye and then their respective cell areas were analyzed by high content profiling platform. The initial cell area of 3 cell types were similar at 0 h time point, while both HET and KO cells showed a delayed phenotype of increasing their cell area when compared with WT cells (Fig. 5B). This observation is independent on the coating material used as the same results were observed when the experiment was performed in fibronectin-coated plate (Fig. S5). Interestingly, HET cells showed the most severe delay in spreading out. These results show that cells with different actin compositions and biophysical features have different ability to stretch the plasma membrane and spread in 2D culture.

3.5. Actin isoforms differentially regulates cellular contractility and protrusion dynamics

To further analyze how the composition of actin isoforms impacts on the mechanical properties of cells, we extended our study using a 3D culture system based on a collagen matrix gel. WT, HET and KO cells were individually mixed with a collagen solution which was then solidified into a gel matrix by neutralizing the pH. 24 h after gel solidification, the 3 cell types displayed striking differences in their morphologies and their respective abilities to contract the gel matrix. Almost all HET cells remained round-shaped and were not able to generate cell protrusions (Fig. 6A, Fig. 6B). About 50% of WT cells could protrude in the collagen matrix, while the percentage significantly increased to 80% in KO cells (Fig. 6B). Compared to WT cells, we found that KO cells tend to have longer protrusions and connect with neighboring protruding cells (Fig. 6A, Fig. 7C). These results suggest that KO cells are more flexible in readjusting their shape and overall morphology in a 3D matrix culture. Consistently, KO cells

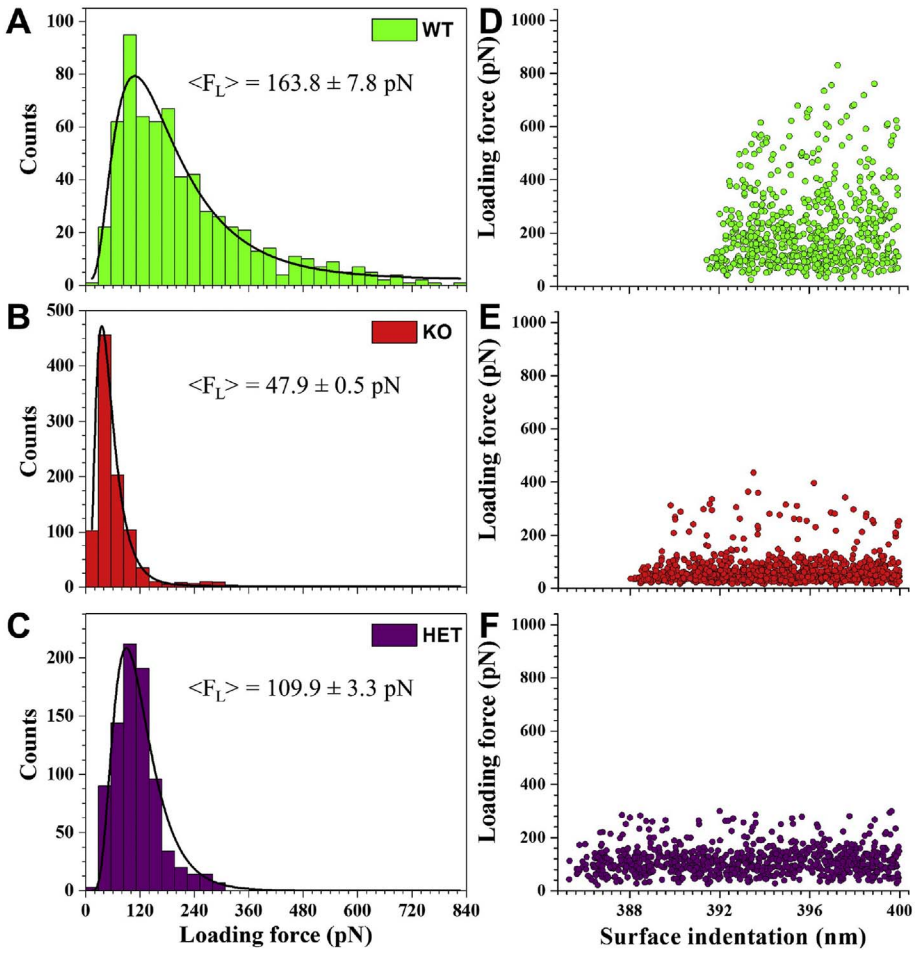

Fig. 3. Loading force and surface indentation measurement. Histograms of the distribution of all loading forces necessary to indent up to 400 nm of the cell surfaces (A–C) and loading force versus surface indentation plots (D–F) measured for WT, KO, and HET cells. Data are pooled results from three independent experiments. Solid black lines are LogNormal fit to data. Values in (A–C) represent mean ± S.D.

showed the greatest ability to contract collagen gel, as reflected by the smallest gel surface area after 48 h culture (Fig. 6C, Fig. 6D). These results suggest that the stronger protrusions produced by KO cells may contribute to enhanced ability to contract the gel matrix.

We further studied the dynamics of protrusion in WT and KO cells. We found that after 6 h post gel formation, > 50% of KO cells already displayed small protrusions while the majority of WT cells still remained round-shaped (Fig. 7A, Fig. 7B). Therefore, KO cells that produce longer protrusions, were also able to generate protrusions much more rapidly than WT cells in collagen gel. Since the establishment of cell protrusions from membranes requires localized actin polymerization [31], we hypothesize that in KO cells the increased rates at which protrusions are generated relies on the constant turnover of F-actin and G-actin. To test this possibility, we cultured WT and KO cells in the presence of the ROCK Kinase inhibitor Y27632, which inhibits actin turnover [32]. We found that the Y27632 compound strongly inhibit the ability of KO cells to contract the collagen gel, while it did not affect WT cells (Fig. 7D). In addition, Y27632 treatment in KO cells led to thinner and distorted protrusions, and impaired cell-cell interactions (Fig. 7E). Therefore, our data shows that rapid actin turnover is essential for the enhanced protrusion formation and ability to contract gel in KO cells.

Taken together, our findings demonstrate that cells with different actin compositions and, consequently, different cell surface biophysical properties have distinct behaviors in 2D and 3D culture environment. It is likely that the changes in the actin cytoskeleton arrangement causes alterations in cell surface stiffness, which contributes to the observed changes in cell spreading and cell protrusion. This is because cell surface can serve as a barrier to antagonize actin-based protrusion from the membrane [33]. On the other hand, contractility of actin fibers can hinder protrusion generation by pulling actin filaments away from the membrane [34].

3.6. Re-introduction of β-actin into KO cells alters cell surface stiffness and pull-off force

To determine whether β-actin has a direct role in the maintenance of surface mechanical properties, we re-introduced β-actin into the KO cells. KO cells were transduced with a retrovirus carrying an HA-tagged β-actin construct (*Actb* cDNA, referred to as KA cells) and with an HA-GFP construct as control (referred to as KG cells) [35]. The viral vector carries rat CD8a surface protein co-expressed with the insert so that cells successfully transduced can be stained with fluorescence-conjugated rat CD8a antibody and sorted by FACS (Fig. 8A). After sorting, cells were allowed to expand and the expression level of re-introduced *Actb* gene was then examined. The KA cells did express *Actb* mRNA, although the level of *Actb* mRNA was quite low compared to the endogenous β-actin mRNA level in WT cells (Fig. 8B). This is because β-actin is one of the most abundantly expressed proteins and it is notoriously difficult to over-express it to the WT level. We next asked how β-actin and smooth muscle alpha actin α-SMA are organized in KA cells by co-staining with anti-HA and anti-SMA antibodies. We found significant co-localization between the re-introduced β-actin and endogenous α-SMA in KA cells, especially within the actin fibers (Fig. 8C),

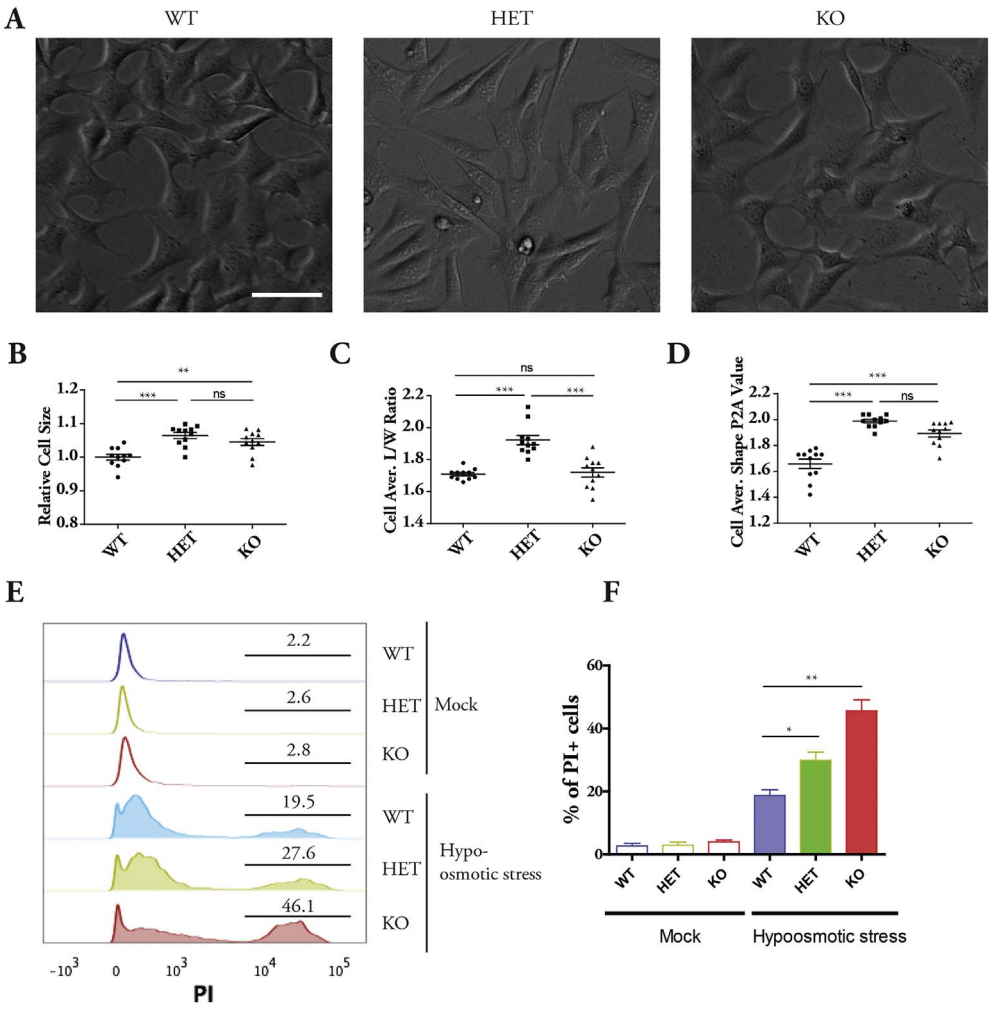

Fig. 4. Cellular morphology and response to hypo-osmotic stress. **A.** Bright field images of cellular morphology of WT, HET and KO MEFs cultured in 6 well plate. Scale bar: 50 μm. (B–D) Cells grown in 96-well plates were fixed and stained with Wheat germ agglutinin (WGA membrane stain) and imaged in ArrayScan XTI high content platform. Cell shape was analyzed using Cellomics compartment analysis package. Cell size, length to width ratio and Perimeter^2/Area ratio (P2A) value were quantified. At least 500 valid single cells were analyzed in each culture wells. Each spot in the data represents the mean value of at least 500 valid single cells in an independent well. Data are pooled results of two independent experiments. (E–F) Culture medium was replaced with sterile H_2O (transient hypo-osmotic stress) or PBS (Mock) for 3 min. Then sterile H_2O was replaced with fresh culture medium for 1 h after medium change. Cells in different groups were stained by PI and analyzed by FACS. Histogram number shows the percentage of PI positive cells with raptured cell membrane. Data are the summary of three independent experiments. Statistics in B, C, D, F: One-way ANOVA analysis with Bonferroni Post Hoc Test: Mean ± S.E.M., (*) $p < 0.05$; (**) $p < 0.01$; (***) $p < 0.001$; ns: not significant.

suggesting that re-introduced β-actin can be incorporated into α-SMA fibers.

We then compared the biophysical properties of KA and KG cells. The distribution of Young's moduli revealed more events with high Young's modulus values detected in KA cells (Fig. 8D, Fig. 8E). Compared to KG cells (56.4 ± 0.9 Pa), the mean cell stiffness of KA cells (85.7 ± 1.7 Pa) increased by 52% (Table 2). Accordingly, the mean loading force needed to indent the cell surfaces of KA cells (68.7 ± 1.0 pN) was higher than that of KG cells (44.3 ± 0.4 pN) (Fig. S6A, Fig. S6B). However, we found that surface indentation range was similar (Fig. S6C, Fig. S6D), indicating no change of cell surface heterogeneity between the 2 cell types. Interestingly, re-introduction of β-actin into KO cells also increased the surface pull-off force to AFM probe (KA cells compared to KG cells). Together, the above findings indicate that changes in the composition of actin through expression of an exogenous β-actin construct in β-actin KO cells can change the biophysical features of cell surface. Particularly, these data suggests that β-actin directly contributes to the surface stiffness of cell.

4. Discussion

In this study, we show that embryonic fibroblasts (MEFs) from β-actin$^{+/+}$ WT, β-actin$^{+/-}$ HET and β-actin$^{-/-}$ KO mice provide altogether a cellular model to study the contribution of β-actin to cell surface biomechanics. Loss of β-actin had no effects on the expression of skeletal or cardiac muscle α-actin, but caused the up-regulation of smooth muscle α-actin (α-SMA) and γ-actin. This is in accordance with previous studies that only a subset of actin isoforms is up-regulated when one isoform is deleted [4], and suggests that to a certain degree smooth muscle α-actin and γ-actin can functionally compensate for the loss of β-actin. Interestingly, varying β-actin dosages can differentially regulate the expression of *Acta2*, *Actg1* and *Actg2* genes among the 3 cell types, creating a cell system in which each cell type has a unique composition of actin isoforms.

Previous studies have shown distinct subcellular localization patterns of certain actin isoforms. For example, cytoplasmic γ-actin appears to evenly distribute in all actin-containing structures in non-muscle cells [36]. In contrast, cytoplasmic β-actin is mainly targeted to the cell periphery [37–40] and this phenomenon is primarily ascribed to the specific localization of the β-actin transcript at plasma membrane [38–40]. This is thought to be mediated by the zipcode-binding protein (ZBP1) that binds to a 54-nucleotide zipcode sequence in the 3′ UTR of β-actin mRNA and facilitates its targeting and translation [38,41]. Consistently, our data showed β-actin fibers are mainly located at cell membrane in WT and HET MEFs. In contrast, in the KO cells lacking β-actin, α-SMA is up-regulated and forms fibers along the cell body, possibly due to its interaction with different groups of actin-binding proteins. In the KO cells, we therefore hypothesize that the depletion of β-actin in the proximity of the plasma membrane affects biophysical properties of cell surface.

In cells, both the intrinsic lipid bilayer tension and cortex cytoskeleton contributes to cell surface biophysical properties [42]. We found that decreasing β-actin levels leads to decrease in cell surface stiffness. The force required to indent the cell surface also decreases with the loss of β-actin levels, indicating that β-actin is essential for maintaining the mechanical strength of cell surface. This seems to be consistent with the

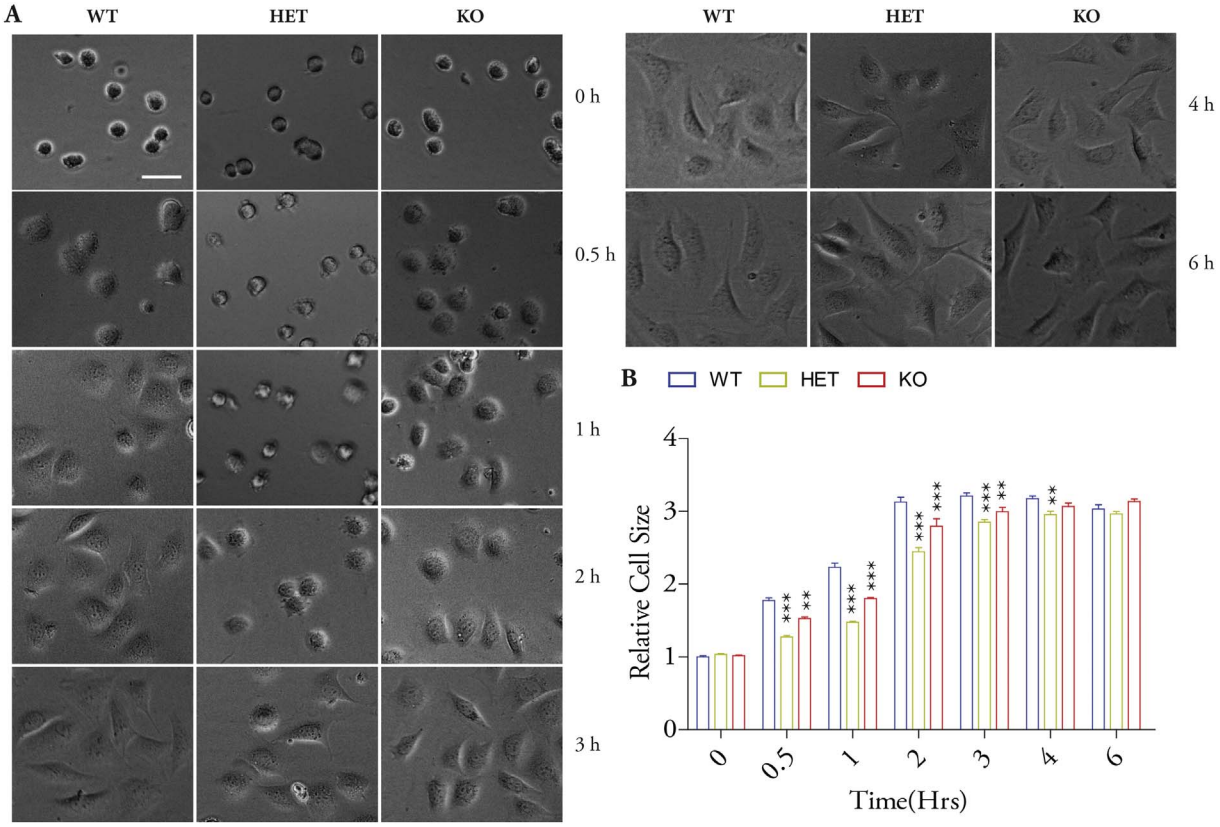

Fig. 5. Cell spreading assay of WT, HET and KO MEFs. **A.** Cells were trypsinized and plated at equal density in 96 well plate. Cells were allowed to settle at the bottom for 15 min (0 h time point) and a time course of cell morphology changes were captured from 0 to 6 h. Scale Bar: 50 μm. **B.** At each time point, cells were fixed and stained with WGA membrane staining dye. Cell size changes were quantified by ArrayScan XTI high content platform. Data are summary of 10 biological replicates. Two-way ANOVA analysis with Bonferroni Post Hoc Test: (**) $p < 0.01$; (***) $p < 0.001$, Mean ± S.E.M. The p values show significance of comparison of HET or KO cells with WT group.

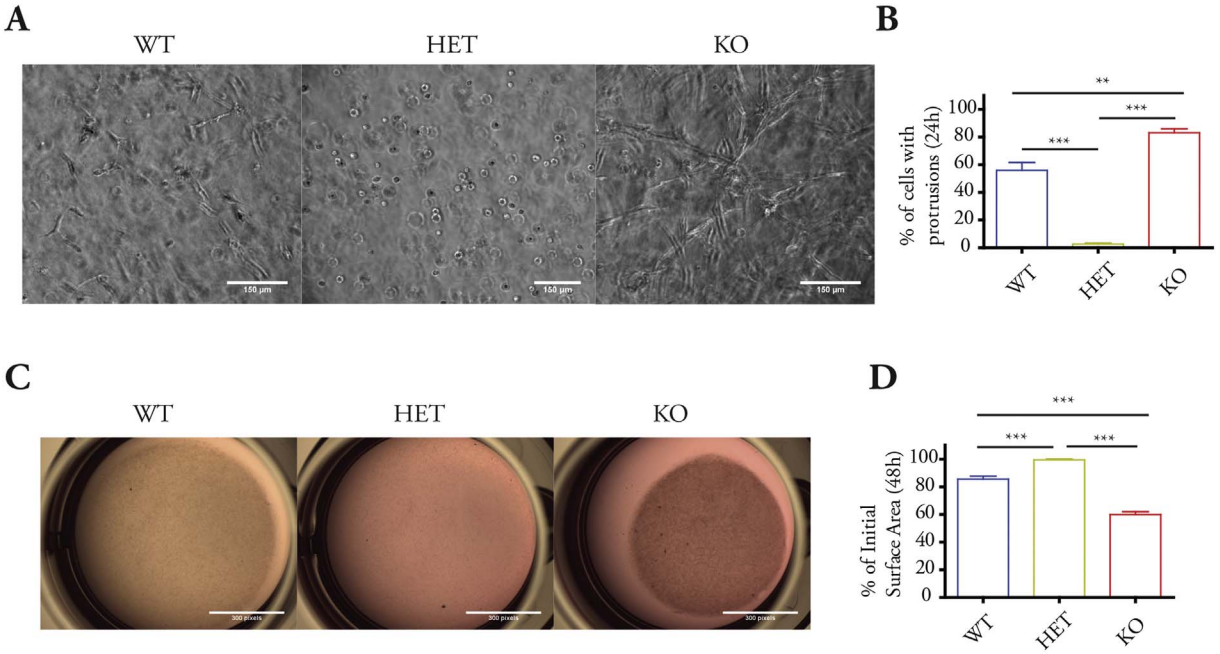

Fig. 6. 3D floating collagen gel culture of MEFs. **A.** Equal number of WT, HET and KO MEFs mixed with collagen gel. The solidified collagen gel was immersed in fresh culture medium. Cell morphology were captured after 24 h post solidification. **B.** Cells displayed extended protrusion in collagen gel matrix were quantified. Data are summary of three independent experiments. One-way ANOVA analysis: (**) $p < 0.01$; (***) $p < 0.001$. **C.** Size of collagen gel were imaged 48 h post solidification. **D.** Summary of gel surface size of 3 independent experiments. One-way ANOVA analysis with Bonferroni Post Hoc Test: (***) $p < 0.001$. Mean ± S.E.M.

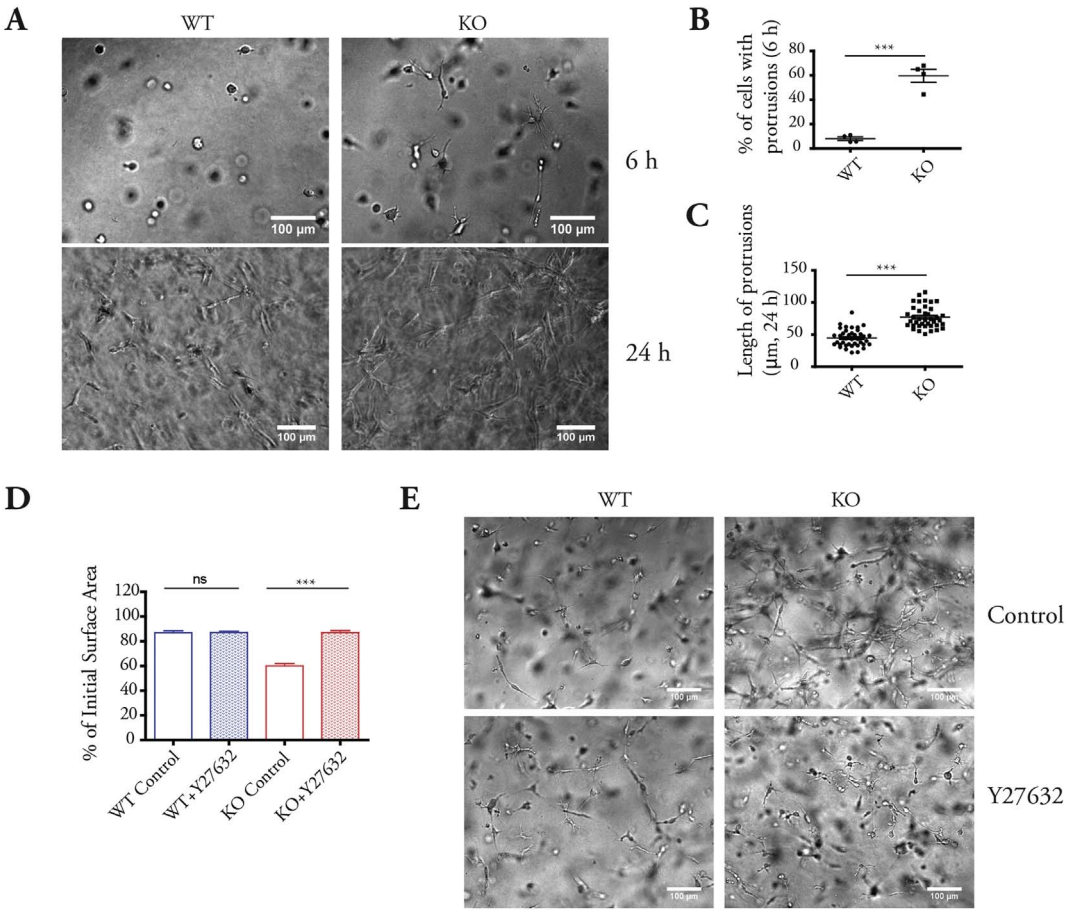

Fig. 7. WT and KO cells show difference in actin dynamic in 3D collagen culture. A. WT and KO MEFs were mixed with collagen gel and the cellular morphology was observed 6 h and 24 h after gel solidification. B. Percentage of cells displaying cell protrusion after 6 h. C. Length of cellular protrusion after 24 h. D. Size of collagen gel were imaged 48 h post solidification with or without Y27632 (4 μM) treatment. E. Cellular morphology in collagen gel with or without Y27632 treatment. All data are the summary of 3 independent experiments. Student's *t*-test: (***) $p < 0.001$. ns: not significant. Mean ± S.E.M.

preferential localization of β-actin at the cell periphery. Compared to HET and KO cells, more β-actin is present at the cell membrane in WT cells. It is, therefore, plausible to conclude that WT cell membrane is more supported and stretched by β-actin-containing structures, which leads to a higher level of surface stiffness. This is further supported by the observation that re-introducing β-actin into KO cells increases its surface stiffness. On the other hand, the massive α-SMA fibers along the cell body increase contractility, which may also contribute to decreasing the cell surface stiffness in KO cells [42]. The enriched β-actin at the membrane and higher degree of membrane stretch may be linked to the narrower range of force induced-indentation of WT cell surface. The decrease in surface stiffness and possible changes in microdomains of the plasma membrane may be contributing factors to the increased pull-off force of HET and KO cells when compared to WT cells [43,44]. It is noteworthy that the KA cells with re-introduced β-actin also showed increased surface pull-off force in comparison to KG cells. This can be explained by the observation that the re-introduced β-actin is incorporated into α-SMA fibers, which may alter the physical property of the existing α-SMA cytoskeleton and the associated surface feature.

Cell surface mechanics such as plasma membrane tension and cortex actin cytoskeleton contribute together to cell shape determination [13,45]. During cell differentiation, actin can undergo reorganization to change cell shape [46]. The different actin contents and varying cell surface mechanical properties can contribute to the difference in cell area and cell shape among WT, HET and KO cells. In response to hypo-osmotic stress, cells increase in volume [15]. To provide sufficient membrane area, cells sacrifice specific membrane domains of protrusions and invaginations such as microvilli and caveolae [15]. Apical actin structures are required to provide mechanical support to those membrane domains [47]. Specifically, a previous study demonstrated that β-actin and its mRNA are enriched at the membrane-cytoskeletal interface within domains of moving cytoplasm [37]. Thus, under hypo-osmotic swelling, the membrane microvilli and caveolae of KO cells without β-actin are possibly more prone to rupture and losing integrity than WT and HET cells.

Notably, WT, HET and KO cells behave quite differently in 2D and 3D cultures. HET cells show the most retarded phenotype in spreading out in 2D culture, and fail to produce protrusions in 3D culture. This may be due to a relative lower amount of total F-actin content compared to WT and KO cells. While KO cells showed delayed rate in spreading in 2D culture compared to WT cells, KO cells are more effective in protrusion generation in 3D culture. This suggests that 2D and 3D environments respectively favor certain actin isoforms and cell surface mechanical features. KO cells expressing smooth muscle α-actin adapt better to 3D culture matrix, as reflected by their ability to more rapidly generate stronger cell protrusions. There is an active debate on the discrepancy of cell behaviors in 2D and 3D culture environment [48]. The adhesion between cell and culture matrix [49], actin cytoskeleton organization [50], cell generated tension [51] and mechanosensing signaling pathways [52] can contribute to different aspects of cell behaviors in a 3D matrix. It is important to note that tension generated by cells embedded in a 3D matrix is a critical factor in regulating cell proliferation, motility, morphology and ECM remodeling [53].

Actin isoforms are critical to provide tissue-specific mechanical properties. Physiological processes such as wound healing also requires the transient expression of smooth muscle α-actin in myofibroblast

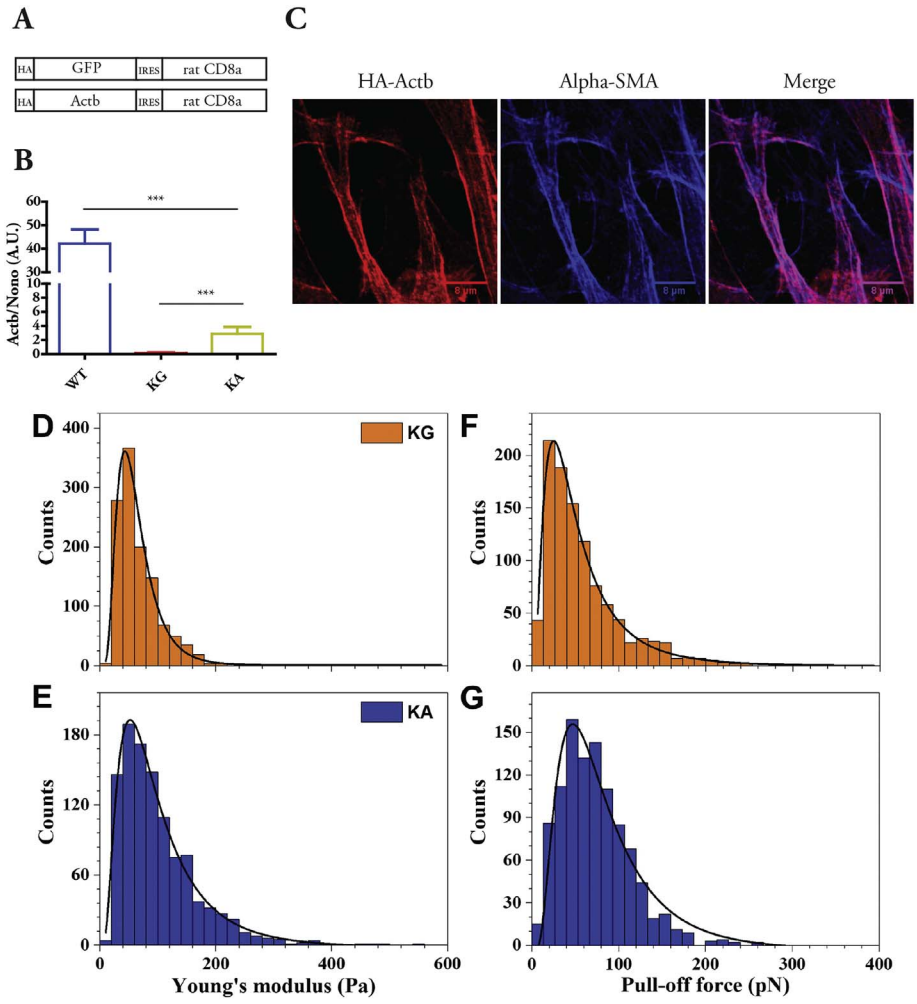

Fig. 8. *Re*-introduction of β-actin into KO cells altered membrane elasticity. A. Schematics of retroviral constructs used to express β-actin. B. qPCR quantification of levels of β-actin mRNA expressed in WT, KG (KO cells transduced with virus carrying HA-GFP) and KA (KO cells transduced with virus carrying HA-Actb). Data are summary of 3 biological replicates. Student's t-test for pairwise comparison: (***) $p < 0.001$, Mean ± S.E.M. C. KA cells were stained with HA and alpha-SMA antibodies and visualized by confocal microscope. Histograms of the distribution of all Young's moduli (D–E) and maximum pull-off force (F–G) measured for KG (KO cells transduced with virus carrying HA-GFP) and KA (KO cells transduced with virus carrying HA-Actb) cells. Solid black lines are LogNormal fit to data.

Table 2
Young's modulus (*E*) and maximum pull-off force (F_P) values for KG and KA MEFs.

Cell type†	Young's modulus		Pull-off force	
	E (Pa)	No. of locations	F_P (pN)	No. of events
KG	56.4 ± 0.9	1174	45.1 ± 0.9	1025
KA	85.7 ± 1.7	1080	71.9 ± 3.2	1026

†: The number of investigated cells were 20 and 18 cells for *KG* and *KA*, respectively. Peak values and standard deviations were derived from distribution histograms by using LogNormal probability density function. For each set of experiment, 64 pairs of force versus displacement curves were acquired from single cells in the force-volume mode. Data represents mean ± S.D.

[54], which imparts specific biophysical properties [55]. Our data support differential localization and organization of different actin isoforms as a mechanism to explain the biophysical properties of cell surface conferred by specific actin isoforms. However, future studies will be necessary to clarify how the mechanical strength of actin isoform fibers and their polymerization/depolymerization rate influence the cell surface mechanics and control cellular activities.

Supplementary data to this article can be found online at https://doi.org/10.1016/j.bbagen.2018.01.021.

Transparency document

The Transparency document associated with this article can be found in online version.

Acknowledgements

We thank Christophe Ampe (University of Gent, Belgium) for kindly providing us with the β-actin$^{+/+}$MEFs, β-actin$^{+/-}$MEFs and the β-actin$^{-/-}$MEFs. This work was supported by grants from New York University Abu Dhabi, the Swedish Research Council (Vetenskapsrådet) and the Swedish Cancer Society (Cancerfonden) to PP. We thank the NYUAD Core Technology Platform (CTP). We are also thankful to the NYUAD CGSB Sequencing and Bioinformatics Core teams for technical support and the computational platform provided by the NYUAD HPC team. The authors would also like to acknowledge support from Science for Life Laboratory, the National Genomics Infrastructure, NGI, and Uppmax for providing assistance in massive parallel sequencing and computational infrastructure.

Conflict of interest

The authors declare no competing financial interests.

References

[1] N.S. Gov, A. Gopinathan, Dynamics of membranes driven by actin polymerization, Biophys. J. 90 (2006) 454–469.
[2] S.H. Lee, R. Dominguez, Regulation of actin cytoskeleton dynamics in cells, Mol. Cells 29 (2010) 311–325.
[3] P.A. Rubenstein, The functional importance of multiple actin isoforms, BioEssays 12 (1990) 309–315.
[4] B.J. Perrin, J.M. Ervasti, The actin gene family: function follows isoform, Cytoskeleton 67 (2010) 630–634.
[5] K.J. Nowak, G. Ravenscroft, C. Jackaman, A. Filipovska, S.M. Davies, E.M. Lim,

S.E. Squire, A.C. Potter, E. Baker, S. Clement, C.A. Sewry, V. Fabian, K. Crawford, J.L. Lessard, L.M. Griffiths, J.M. Papadimitriou, Y. Shen, G. Morahan, A.J. Bakker, K.E. Davies, N.G. Laing, Rescue of skeletal muscle alpha-actin-null mice by cardiac (fetal) alpha-actin, J. Cell Biol. 185 (2009) 903–915.
[6] M.A. Jaeger, K.J. Sonnemann, D.P. Fitzsimons, K.W. Prins, J.M. Ervasti, Context-dependent functional substitution of alpha-skeletal actin by gamma-cytoplasmic actin, FASEB J. 23 (2009) 2205–2214.
[7] C. Ampe, M. Van Troys, Mammalian actins: isoform-specific functions and diseases, Handb. Exp. Pharmacol. 235 (2017) 1–37.
[8] E. Heller, E. Fuchs, Tissue patterning and cellular mechanics, J. Cell Biol. 211 (2015) 219–231.
[9] D. Wang, W. Zheng, Y. Xie, P. Gong, F. Zhao, B. Yuan, W. Ma, Y. Cui, W. Liu, Y. Sun, M. Piel, W. Zhang, X. Jiang, Tissue-specific mechanical and geometrical control of cell viability and actin cytoskeleton alignment, Sci. Rep. 4 (2014) 6160.
[10] F. Lautenschlager, S. Paschke, S. Schinkinger, A. Bruel, M. Beil, J. Guck, The regulatory role of cell mechanics for migration of differentiating myeloid cells, Proc. Natl. Acad. Sci. U. S. A. 106 (2009) 15696–15701.
[11] T. Lecuit, P.F. Lenne, Cell surface mechanics and the control of cell shape, tissue patterns and morphogenesis, Nat. Rev. Mol. Cell Biol. 8 (2007) 633–644.
[12] R. Magno, V.A. Grieneisen, A.F. Maree, The biophysical nature of cells: potential cell behaviours revealed by analytical and computational studies of cell surface mechanics, BMC Biophys. 8 (2015) 8.
[13] G. Salbreux, G. Charras, E. Paluch, Actin cortex mechanics and cellular morphogenesis, Trends Cell Biol. 22 (2012) 536–545.
[14] E.K. Paluch, C.M. Nelson, N. Biais, B. Fabry, J. Moeller, B.L. Pruitt, C. Wollnik, G. Kudryasheva, F. Rehfeldt, W. Federle, Mechanotransduction: use the force(s), BMC Biol. 13 (2015) 47.
[15] A. Pietuch, B.R. Bruckner, A. Janshoff, Membrane tension homeostasis of epithelial cells through surface area regulation in response to osmotic stress, BBA-Mol. Cell Res. 1833 (2013) 712–722.
[16] A.D. Lieber, S. Yehudai-Resheff, E.L. Barnhart, J.A. Theriot, K. Keren, Membrane tension in rapidly moving cells is determined by cytoskeletal forces, Curr. Biol. 23 (2013) 1409–1417.
[17] L. Bo, R.E. Waugh, Determination of bilayer-membrane bending stiffness by pull-off formation from Giant, thin-walled vesicles, Biophys. J. 55 (1989) 509–517.
[18] N.C. Gauthier, M.A. Fardin, P. Roca-Cusachs, M.P. Sheetz, Temporary increase in plasma membrane tension coordinates the activation of exocytosis and contraction during cell spreading, Proc. Natl. Acad. Sci. U. S. A. 108 (2011) 14467–14472.
[19] B. Pontes, N.B. Viana, L.T. Salgado, M. Farina, V.M. Neto, H.M. Nussenzveig, Cell cytoskeleton and tether extraction, Biophys. J. 101 (2011) 43–52.
[20] N.C. Gauthier, O.M. Rossier, A. Mathur, J.C. Hone, M.P. Sheetz, Plasma membrane area increases with spread area by exocytosis of a GPI-anchored protein compartment, Mol. Biol. Cell 20 (2009) 3261–3272.
[21] D. Tondeleir, A. Lambrechts, M. Muller, V. Jonckheere, T. Doll, D. Vandamme, K. Bakkali, D. Waterschoot, M. Lemaistre, O. Debeir, C. Decaestecker, B. Hinz, A. Staes, E. Timmerman, N. Colaert, K. Gevaert, J. Vandekerckhove, C. Ampe, Cells lacking beta-actin are genetically reprogrammed and maintain conditional migratory capacity, Mol. Cell. Proteomics 11 (2012) 255–271.
[22] J.L. Hutter, J. Bechhoefer, Calibration of atomic-force microscope tips, Rev. Sci. Instrum. 64 (1993) 1868–1873.
[23] Z.Y. Suo, R. Avci, M. Deliorman, X.H. Yang, D.W. Pascual, Bacteria survive multiple puncturings of their cell walls, Langmuir 25 (2009) 4588–4594.
[24] E.K. Dimitriadis, F. Horkay, J. Maresca, B. Kachar, R.S. Chadwick, Determination of elastic moduli of thin layers of soft material using the atomic force microscope, Biophys. J. 82 (2002) 2798–2810.
[25] N.I. Abu-Lail, T.A. Camesano, Specific and nonspecific interaction forces between *Escherichia coli* and silicon nitride, determined by Poisson statistical analysis, Langmuir 22 (2006) 7296–7301.
[26] M.Z. Sun, J.S. Graham, B. Hegedus, F. Marga, Y. Zhang, G. Forgacs, M. Grandbois, Multiple membrane tethers probed by atomic force microscopy, Biophys. J. 89 (2005) 4320–4329.
[27] X. Xie, M.J.T. Stubbington, J.K. Nissen, K.G. Andersen, D. Hebenstreit, S.A. Teichmann, A.G. Betz, The regulatory T cell lineage factor Foxp3 regulates gene expression through several distinct mechanisms mostly independent of direct DNA binding, PLoS Genet. 11 (2015) e1005251.
[28] B.J. Perrin, K.J. Sonnemann, J.M. Ervasti, Beta-actin and gamma-actin are each dispensable for auditory hair cell development but required for stereocilia maintenance, PLoS Genet. 6 (2010) e1001158.
[29] D. Shmerling, C.P. Danzer, X.H. Mao, J. Boisclair, M. Haffner, M. Lemaistre, V. Schuler, E. Kaeslin, R. Korn, K. Burki, B. Ledermann, B. Kinzel, M. Muller, Strong and ubiquitous expression of transgenes targeted into the beta-actin locus by cre/lox cassette replacement, Genesis 42 (2005) 229–235.
[30] E. Paluch, C.P. Heisenberg, Biology and physics of cell shape changes in development, Curr. Biol. 19 (2009) R790–R799.
[31] R. Ananthakrishnan, A. Ehrlicher, The forces behind cell movement, Int. J. Biol. Sci. 3 (2007) 303–317.
[32] S. Escuin, B. Vernay, D. Savery, C.B. Gurniak, W. Witke, N.D.E. Greene, A.J. Copp, Rho-kinase-dependent actin turnover and actomyosin disassembly are necessary for mouse spinal neural tube closure, J. Cell Sci. 128 (2015) 2468–2481.
[33] K. Keren, Z. Pincus, G.M. Allen, E.L. Barnhart, G. Marriott, A. Mogilner, J.A. Theriot, Mechanism of shape determination in motile cells, Nature 453 (2008) [475-U471].
[34] O.O. Marchenko, S. Das, J. Yu, I.L. Novak, V.I. Rodionov, N. Efimova, T. Svitkina, C.W. Wolgemuth, L.M. Loew, A minimal actomyosin-based model predicts the dynamics of filopodia on neuronal dendrites, Mol. Biol. Cell 28 (2017) 1021–1033.
[35] X. Xie, B. Almuzzaini, N. Drou, S. Kremb, A. Yousif, A.O. Farrants, K. Gunsalus, P. Percipalle, Beta-actin-dependent global chromatin organization and gene expression programs control cellular identity, FASEB J. (2017), http://dx.doi.org/10.1096/fj.201700753R.
[36] C.A. Otey, M.H. Kalnoski, J.L. Lessard, J.C. Bulinski, Immunolocalization of the gamma-isoform of nonmuscle actin in cultured-cells, J. Cell Biol. 102 (1986) 1726–1737.
[37] T.C. Hoock, P.M. Newcomb, I.M. Herman, Beta actin and its mRNA are localized at the plasma membrane and the regions of moving cytoplasm during the cellular response to injury, J. Cell Biol. 112 (1991) 653–664.
[38] E.H. Kislauskis, X.C. Zhu, R.H. Singer, Sequences responsible for intracellular-localization of beta-actin messenger-Rna also affect cell phenotype, J. Cell Biol. 127 (1994) 441–451.
[39] E.A. Shestakova, R.H. Singer, J. Condeelis, The physiological significance of beta-actin mRNA localization in determining cell polarity and directional motility, Proc. Natl. Acad. Sci. U. S. A. 98 (2001) 7045–7050.
[40] M.A. Hill, P. Gunning, Beta and gamma actin mRNAs are differentially located within myoblasts, J. Cell Biol. 122 (1993) 825–832.
[41] J. Condeelis, R.H. Singer, How and why does beta-actin mRNA target? Biol. Cell. 97 (2005) 97–110.
[42] A. Diz-Munoz, D.A. Fletcher, O.D. Weiner, Use the force: membrane tension as an organizer of cell shape and motility, Trends Cell Biol. 23 (2013) 47–53.
[43] K. Sengupta, L. Limozin, Adhesion of soft membranes controlled by tension and interfacial polymers, Phys. Rev. Lett. 104 (2010) 088101.
[44] S. Hakomori, Membrane microdomains defining cell adhesion and signaling, Trends Glycosci. Glyc. 13 (2001) 219–230.
[45] P. Rangamani, G.Y. Xiong, R. Iyengar, Multiscale modeling of cell shape from the actin cytoskeleton, Prog. Mol. Biol. Transl. Sci. 123 (2014) 143–167.
[46] K.J. Chalut, E.K. Paluch, The actin cortex: a bridge between cell shape and function, Dev. Cell 38 (2016) 571–573.
[47] L. Figard, M.Y. Wang, L.L. Zheng, I. Golding, A.M. Sokac, Membrane supply and demand regulates F-actin in a cell surface reservoir, Dev. Cell 37 (2016) 267–278.
[48] M.A. Schwartz, C.S. Chen, Deconstructing dimensionality, Science 339 (2013) 402–404.
[49] E. Cukierman, R. Pankov, D.R. Stevens, K.M. Yamada, Taking cell-matrix adhesions to the third dimension, Science 294 (2001) 1708–1712.
[50] U.S. Schwarz, M.L. Gardel, United we stand - integrating the actin cytoskeleton and cell-matrix adhesions in cellular mechanotransduction, J. Cell Sci. 125 (2012) 3051–3060.
[51] R.A. Brown, R. Prajapati, D.A. McGrouther, I.V. Yannas, M. Eastwood, Tensional homeostasis in dermal fibroblasts: mechanical responses to mechanical loading in three-dimensional substrates, J. Cell. Physiol. 175 (1998) 323–332.
[52] D.E. Ingber, Cellular mechanotransduction: putting all the pieces together again, FASEB J. 20 (2006) 811–827.
[53] F. Grinnell, W.M. Petroll, Cell motility and mechanics in three-dimensional collagen matrices, Ann. Rev. Cell Dev. Biol. 26 (2010) 335–361.
[54] I. Darby, O. Skalli, G. Gabbiani, Alpha-smooth muscle actin is transiently expressed by myofibroblasts during experimental wound-healing, Lab. Investig. 63 (1990) 21–29.
[55] B. Li, J.H.C. Wang, Fibroblasts and myofibroblasts in wound healing: force generation and measurement, J. Tissue Viability 20 (2011) 108–120.